

## Article

# Co-Estimating State of Charge and Capacity of Automotive Lithium-Ion Batteries Under Deep Degradation Using Multiple Estimators

Min Young Yoo <sup>1</sup>, Jung Heon Lee <sup>2</sup> , Hyunjoon Lee <sup>2</sup> , Joo-Ho Choi <sup>3</sup> , Jae Sung Huh <sup>4</sup> and Woosuk Sung <sup>5,\*</sup>

<sup>1</sup> Department of Aerospace & Mechanical Engineering, Korea Aerospace University, Goyang-si 10540, Gyeonggi-do, Republic of Korea; myyoo@kau.kr

<sup>2</sup> Department of Smart Air Mobility, Korea Aerospace University, Goyang-si 10540, Gyeonggi-do, Republic of Korea; dlwjdgs95@naver.com (J.H.L.); moon0601jk@kau.kr (H.L.)

<sup>3</sup> School of Aerospace & Mechanical Engineering, Korea Aerospace University, Goyang-si 10540, Gyeonggi-do, Republic of Korea; jhchoi@kau.ac.kr

<sup>4</sup> Aerospace Propulsion Division, Korea Aerospace Research Institute, Yuseong-Gu, Daejeon 3411, Republic of Korea; jshuh@kari.re.kr

<sup>5</sup> School of Mechanical System and Automotive Engineering, Chosun University, Gwangju 61452, Republic of Korea

\* Correspondence: wsung@chosun.ac.kr

**Abstract:** Since battery systems typically account for over 40% of the cost of an electric vehicle, their mid-life replacements are exceptional. Therefore, the battery's lifespan must exceed that of the vehicle. To ensure long-term and safe use, accurate state-of-charge (SOC) estimation must be maintained throughout the battery's lifespan. This requires appropriate updates to parameters, such as capacity, in the battery model. In this context, dual extended Kalman filters, which simultaneously estimate both states and parameters, have gained interest. While existing reports on simultaneous estimators seemed promising, our study found that they performed well under low levels of battery aging but encountered issues at higher levels. Accurately reflecting the actual physicochemical changes of the parameters in aging cells is challenging for two reasons: the limited number of measurements of terminal voltage available for numerous parameters, and the weak observability of the capacity. Therefore, we combined the simultaneous estimator with a capacity estimator operated separately during charging and a sequential estimator specialized for an enhanced self-correcting model, achieving SOC accuracy within 5% even when the SOH decreased by 30%. However, there is still much work to be carried out to implement sequential estimators in battery management systems operating in real time with limited computational resources.

**Keywords:** lithium-ion battery; battery management system; battery aging; enhanced self-correcting model; dual extended Kalman filter; state of charge; capacity



**Citation:** Yoo, M.Y.; Lee, J.H.; Lee, H.; Choi, J.-H.; Huh, J.S.; Sung, W. Co-Estimating State of Charge and Capacity of Automotive Lithium-Ion Batteries Under Deep Degradation Using Multiple Estimators. *Appl. Sci.* **2024**, *14*, 9569. <https://doi.org/10.3390/app14209569>

Academic Editors: Na Li and Lei Li

Received: 15 August 2024

Revised: 29 September 2024

Accepted: 7 October 2024

Published: 20 October 2024



**Copyright:** © 2024 by the authors. Licensee MDPI, Basel, Switzerland. This article is an open access article distributed under the terms and conditions of the Creative Commons Attribution (CC BY) license (<https://creativecommons.org/licenses/by/4.0/>).

## 1. Introduction

Lithium-ion batteries (LIBs) have been extensively applied in various fields, highlighting their critical role in future energy sustainability [1]. Among these applications, road transportation is where LIBs have the greatest impact. While LIBs play a critical role in electric vehicles, the aging of these batteries presents significant challenges for end-of-life management. Retired batteries that no longer meet the requirements must be urgently addressed to prevent safety issues [2]. For the reliable use of LIBs in electric vehicles, developing an advanced battery management system (BMS) for accurately estimating battery states is essential [3]. Research in this area has become increasingly prominent in recent years, with a significant rise in publications focusing on state-of-charge (SOC) estimation [4–7].

Although directly measuring SOC based on Coulomb counting is possible, achieving high accuracy requires dedicated current sensors, which can be as costly as USD 1000. Such sensors are unaffordable for commercial BMSs that are under significant cost pressure. Therefore, inexpensive but reliable estimation methods are required. Despite being estimates, the SOC must be as accurate as measurements obtained from current sensors enhanced with internal compensation. For use in electric vehicles, an SOC error within 5% over the full range is targeted.

Among estimation methods, Kalman filters (KFs) have proven particularly effective, with more than half of model-based SOC estimators relying on KFs and their variants [4]. Notwithstanding the widespread use of Kalman filtering, estimating the SOC for aged batteries remains challenging, as it requires the concurrent estimation of SOC and capacity [8–10]. Despite the strong correlation between SOC and capacity, existing methods typically estimate them separately, resulting in relatively limited comprehensive investigations into their simultaneous estimation [11]. Even when simultaneous estimation is explored, new or minimally used batteries are typically applied [12–25]. This gap in research limits the development of BMSs for electric vehicles, where state estimation accuracy must be maintained throughout the battery's lifespan. Besides KFs, alternative approaches such as using ultrasonic reflection waves for state-of-charge and temperature joint estimation have also been reported. In this method, a piezoelectric transducer attached to the battery surface transmits ultrasonic signals, allowing for the real-time monitoring of internal battery conditions in a non-destructive manner [26].

Depending on how states and parameters in a battery model are estimated and updated, KFs are divided into two main groups. The first group uses a single filter to estimate states, with parameters updated separately through an optimization technique [27–30]. However, this method is burdened by higher computational demands due to the execution of two separate implementations. Determining the frequency of parameter updates can be another challenge in this method. The second group uses a dual filter for simultaneous state estimation and parameter updating [31–35]. Robust Kalman filtering techniques, such as those presented in [36], emphasize the strength of the dual extended Kalman filter (DEKF) in addressing model uncertainties, enhancing robustness and accuracy in state and parameter estimation. While this method allows for more comprehensive investigations of battery aging, it poses significant challenges due to the complexity of the variables involved. This complexity is further compounded by the limited number of direct measurements, namely, terminal voltage compared to the number of estimates. Consequently, the limited measurements can lead to less accurate estimations of battery states and parameters, affecting the reliability of the overall BMS and its decisions.

The co-estimation of SOC and capacity using a dual filter requires discussion in terms of various aspects: the types of battery models, the types of filters used to estimate states and parameters in the model, the specific settings of the filter, and the degree of battery degradation. Firstly, Thevenin models are most widely adopted, such as first-order (1RC) [31], second-order (2RC) [32,33], and fractional second-order [34,35] models. While extended Kalman filters (EKFs) are commonly employed, variants such as unscented Kalman filters (UKFs) [30] or adaptive extended Kalman filters (AEKFs) [27] are sometimes used. In some cases [31,35], the filters operate at different time intervals to account for the distinct characteristics of state and parameter estimations. The filter must be initially set, but the values of error, process noise, and measurement noise covariances are not often specified [33,35]. Aged batteries are required for the filter to yield estimation results, and their degradation levels should preferably be wide and regular—for example, test data prepared at uniform intervals of 5% across the entire range of 30% in capacity fade—but unfortunately, they are not [27,28,31,33,35]. In addition, despite using Kalman filtering, estimation results are often provided without confidence intervals. The summarized discussion from the aforementioned studies is presented in Table 1. Tracking performance is typically evaluated by deliberately initializing the filter with incorrect state and parameter values, then measuring the convergence time and steady-state error. Each study claims

superiority based solely on the steady-state error, generally measured by root mean square error (RMSE). However, in prior studies, filters have differed in structure, initialization, and covariance settings, and test data vary in battery degradation level and load profile. Such result-oriented information is insufficient to comprehensively assess the performance and validity of the previously reported estimators and to clearly understand them. Consequently, despite the abundance of prior studies, they are not readily applicable to practical BMS developments.

**Table 1.** Prior studies on the co-estimation of SOC and capacity using a dual filter for aged batteries.

Ref.	Battery Model (Thevenin)	Filter (State Parameters)	Estimates (State Parameters)	Level of Aging [%] (Equation to SOH)	Notes
[31]	1RC	EKF EKF (multi-scale)	SOC All parameters	97.5	
				90.3	
				80	
				70.3	
[32]	2RC	EKF EKF	SOC Capacity, Resistance	100	
				97	
				85	
				78	
[33]	2RC	AEKF KF	SOC Resistance	96.5	Adaptive EKFs
				94	
				92.45	
[34]	Fractional 2RC	FOEKF FOEKF	SOC Capacity, Resistance	93	Fractional-Order EKFs
				88.2	
				80.4	
[35]	Fractional 2RC	FOMIUKF UKF (multi-scale)	SOC Capacity, Resistance	98.1	Fractional-Order Multi-Innovation UKFs
				94.7	
				91.5	

With these drawbacks in mind, our methodology for co-estimating the SOC and capacity is presented in this paper, with an emphasis on validating the developed estimators against abundant test data. Test data are crucial for identifying model parameters and validating state estimates. In this study, we extensively use as many as 30 datasets. These datasets are generated from three load profiles typically applied to modern plug-in hybrid electric vehicles (PHEVs). Nearly 30% capacity degradation is realized in the datasets, which is relatively evenly distributed across ten levels. An enhanced self-correcting (ESC) model, the augmented Thevenin model with a hysteresis element, is applied to a DEKF. This filter updates parameters in the model, ensuring that the model maintains its accuracy in estimating states regardless of battery aging.

## 2. Cell Testing

This section describes the test data generated to identify parameters in a battery model by using a fresh cell. The cell was then cycled to produce battery aging test data, which were used to trace changes in parameters and states with the developed cell model and its filter.

We generally followed the test conditions used in our prior study [37]. We utilized a LIB cell (Samsung SDI, 18650-35E) with a nominal capacity of 3.5 Ah and a nominal voltage of 3.7 V. The load profiles were simulated by combining a DC electronic load (Kikusui, PLZ1004W) and a DC power supply (Kikusui, PWR800L). Seamless transitions between charging and discharging in the load profiles were achieved by integrating these devices with a charge–discharge system controller (Kikusui, PFX2512). Previously, we estimated current sensor bias to study its effect on SOC estimation, as the bias is a well-known source

of process noise affecting the reliability of the SOC. Since the bias is not subject to change with battery aging, only a fresh cell was used. However, this study requires aged cells with reduced capacity to investigate the impact of capacity variations on SOC estimation. For this purpose, the cell was intentionally aged through continuous cycling, as depicted in Figure 1b. Each cycle involved a constant current charge at 2 C-rate until the voltage reached 4.2 V, followed by a constant voltage charge at this level until the current dropped to 1 A. After resting for an hour, the cycle proceeded with a constant current discharge at 2 C-rate until the voltage fell to 2.5 V. This high current, applied over a wide SOC range, accelerated capacity loss. Before starting this cycle test, the cell was evaluated through an initial reference performance test (RPT), as shown in Figure 1a. The test was repeated every 100 cycles up to cycle 300, and then every 300 cycles up to cycle 2100. The test was designed to mimic the real-world operations of PHEVs, as described below. First, the batteries in the vehicle are plugged in to charge. The electrical energy stored in the batteries is then used to propel the vehicle, gradually depleting SOC. This mode is thus referred to as the charge-depleting (CD) operation. When the available electrical energy in the batteries is almost depleted, the vehicle transitions to charge-sustaining (CS) mode. In this mode, the SOC is stabilized as the vehicle mainly utilizes the internal combustion engine for propulsion. The vehicle remains in this mode until the batteries are reconnected for recharging. In this study, three different but representative CD and CS operations were employed as load profiles: the City, Highway, and High-speed profiles represent stop-and-go city, highway, and aggressive highway driving, respectively. Unlike in the City and Highway profiles, CS is not included in the High-speed profile. In accordance with the prescribed operation of PHEVs, the test consisted of a constant power charge at 9 W until the SOC reached 90%, an hour rest, and a dynamic current discharge and charge until the SOC reached approximately 15%. At this level of SOC, transitioning from CD to CS occurred during both the City and Highway profiles.

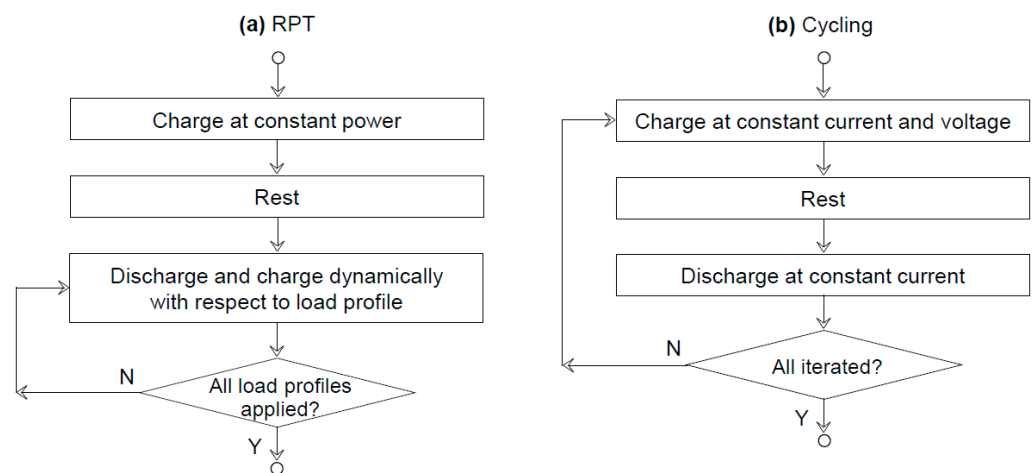


**Figure 1.** Cell testing schedule consisting of (a) RPT conducted before and during (b) cycling.

A total of 30 datasets were finally obtained from the three load profiles with ten tests performed at cycles 0, 100, 200, 300, 600, 900, 1200, 1500, 1800, and 2100. As a result, Figure 2 plots changes in the rated capacity, which decreases almost linearly per cycle, except at cycle 1500. At the final cycle, the capacity was measured to be 2.254 Ah. This final capacity corresponds to about 70% state of health (SOH), as it represents the present capacity relative to a nominal capacity of 3.23 Ah. This level of SOH falls below the end-of-life threshold for batteries in currently sold electric vehicles. Figure 3 plots changes in the terminal voltage and SOC as capacity decreases. Due to space constraints, the measurement results from four specific cycles (0, 300, 1200, and 2100) are selectively presented. For each cycle, the three load profiles were applied to aging cells, and the initial SOC was set to 90%. As

capacity decreased, cycles later than 300 were subject to abrupt termination due to rapidly reaching a cut-off voltage of 2.5 V.

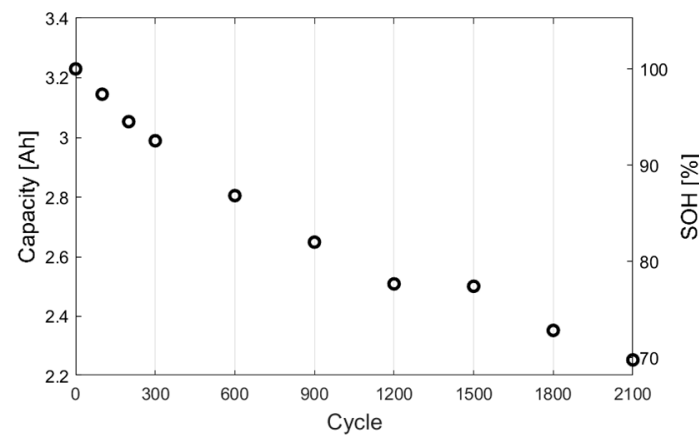


**Figure 2.** Variations in capacity measurements over cycles.

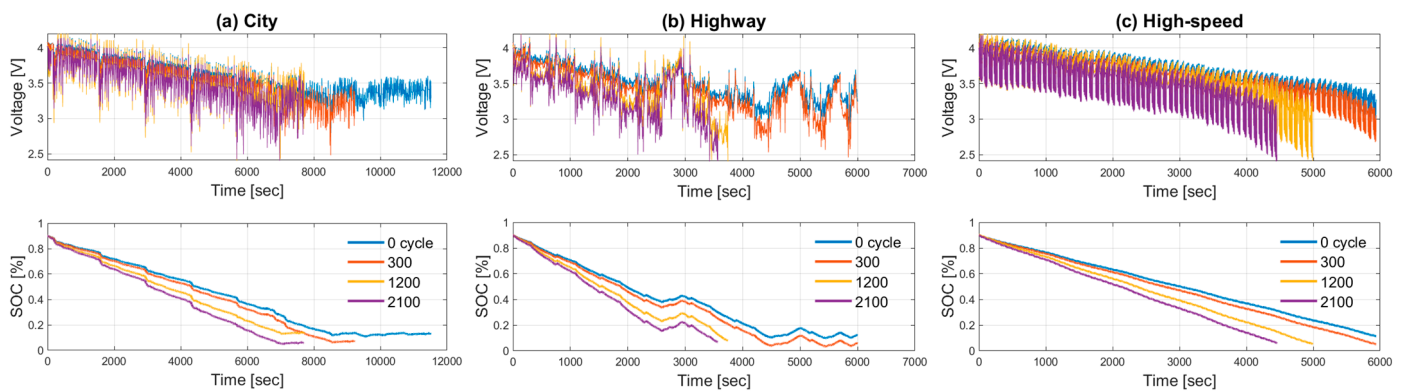


**Figure 3.** Variations in terminal voltage and SOC measurements over time under the (a) City, (b) Highway, and (c) High-speed profiles, representing stop-and-go city, highway, and aggressive highway driving, respectively.

### 3. Cell Modeling

This section formulates a cell model and identifies its parameters that can predict the terminal voltage despite battery aging.

We compared a typical Thevenin model to its variant, an enhanced self-correcting (ESC) model [38], and selected the model with higher fidelity to the test data acquired from aged cells. The Thevenin model is one of the most widely utilized equivalent circuit models for battery state estimation, representing the time-dependent polarization voltages using one or more parallel resistor–capacitor (RC) elements. The ESC model extends the Thevenin model with an additional element that can describe the SOC-varying and instantaneous hysteresis voltages. These models were developed through an evolutionary process, progressively integrating states and their relevant parameters. Basically, the output voltage  $v_T$  was predicted based on the input current  $i$  flowing through the ohmic resistance  $R_0$ . The states for the SOC  $z$  and the current  $i_{R_j}$  flowing through the polarization resistance  $R_j$  paired with capacitance  $C_j$  were incorporated, building the Thevenin model. To complete the ESC model in Figure 4, a state for the hysteresis voltage  $h$  was added, using the instantaneous hysteresis voltage  $s$  as an input.



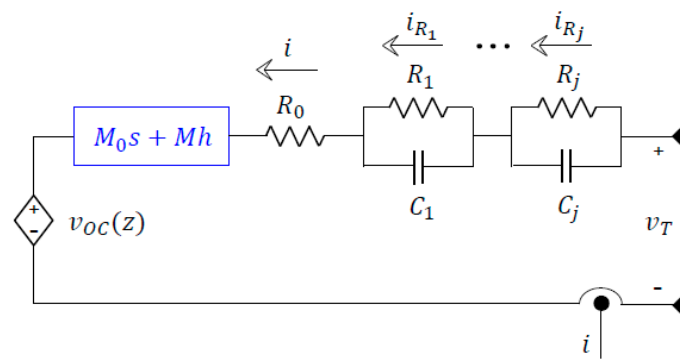


**Figure 4.** Circuit schematic for the ESC model, which is almost the same as the Thevenin model, except for the addition of hysteresis voltages (shown in blue).

As detailed in our previous study [37], the model parameters were identified sequentially. Rather than identifying all parameters at once, the time constant  $\tau_j$  was directly solved using suboptimal linear optimization. Based on the initial guess of the decay rate of hysteresis  $\gamma$ , the states were computed. Subsequently, the maximum hysteresis  $M$ , the maximum instantaneous hysteresis  $M_0$ ,  $R_0$ , and  $R_j$  were iteratively solved by non-negative least-squares. Finally,  $\gamma$  was updated iteratively. This sophisticated method, referred to as a sequential estimator in this study, allows for effectively estimating many parameters with only one measurement,  $v_T$ . In consequence, a total of 12 cases were created by applying the three load profiles to the four cell models. Both models utilize either one or two RC elements, referred to as Thevenin 1RC, Thevenin 2RC, ESC 1RC, and ESC 2RC. These models are named according to the load profiles applied during cell modeling. For instance, a Thevenin or ESC model developed using the High-speed profile is referred to as the High-speed model in this context. The load profiles used include City, Highway, and High-speed.

Figure 5 plots changes in the error between the measured and predicted terminal voltages, comparing modeling accuracy across the type of load profiles, the type of cell models, and the number of cycles. First, regarding the effect of load type, the error exhibits no appreciable difference among them. The High-speed models operating solely in CD mode produce RMSEs similar to those achieved by the City or Highway models, which operate in both CD and CS modes. Regarding the effect of cycle number, the error generally increases with decreasing capacity, irrespective of load and model types. This observation can be accounted for by limitations in representing the physicochemical changes in aged cells. Regarding the effect of model type, the ESC models evidently outperform the Thevenin models in predicting the terminal voltage. The ESC model maintains higher accuracy throughout all of the cycles due to the incorporation of the hysteresis voltage state and its associated parameter. Here, hysteresis refers to the phenomenon where SOC is prone to a lagging effect based on previous charging and discharging. The original intention of integrating the hysteresis element is to improve SOC accuracy by modeling this phenomenon; however, unintended advantages occurred. One of the main reasons for the increasing error is irreversible changes in the SOC–open circuit voltage (OCV) curve. The ESC model is more robust to this change because its hysteresis element allows for some adjustment of the curve over time. To support this claim, the difference in the error between the Thevenin and ESC models is not significantly large in the earlier cycles, but it gradually increases when approaching later cycles. This observation can be interpreted as the curve remaining intact during the early cycles, when battery aging is minimal. Another observation regarding the effect of model type is that the addition of RC elements significantly enhances the Thevenin model but does not improve the ESC model. This discrepancy arises because the hysteresis element reduces the relative influence of additional RC elements in the ESC model. Therefore, integrating the hysteresis element is more helpful in creating a cell model with greater fidelity, compared to simply increasing

the number of RC elements. In consequence, we selected the ESC 1RC as the optimal model type. The state and output equations of the selected model are formulated as:

$$\begin{bmatrix} z_k \\ i_{R_1,k} \\ h_k \end{bmatrix} = \begin{bmatrix} 1 & 0 & 0 \\ 0 & e^{-\frac{\Delta t}{R_1 C_1}} & 0 \\ 0 & 0 & e^{-|\frac{\eta i_{k-1} \gamma \Delta t}{Q}|} \end{bmatrix} \begin{bmatrix} z_{k-1} \\ i_{R_1,k-1} \\ h_{k-1} \end{bmatrix} + \begin{bmatrix} -\frac{\eta \Delta t}{Q} & 0 \\ 1 - e^{-\frac{\Delta t}{R_1 C_1}} & 0 \\ 0 & e^{-|\frac{\eta i_{k-1} \gamma \Delta t}{Q}|} - 1 \end{bmatrix} \begin{bmatrix} i_{k-1} \\ \text{sign}(i_{k-1}) \end{bmatrix} + \omega_{k-1} \quad (1)$$

$$v_{T,k} = \text{OCV}(z_k) + M_0 \text{sign}(i_k) + M h_k - R_1 i_{R_1,k} - R_0 i_k + v_k \quad (2)$$

where  $k$  is the integer time index,  $\Delta t$  is the measurement time interval,  $\eta$  is the coulombic efficiency, and  $Q$  is capacity. The three states  $z$ ,  $i_{R_1}$ , and  $h$  are involved, along with the seven parameters  $Q$ ,  $\tau$ ,  $M$ ,  $M_0$ ,  $R_0$ ,  $R_1$ , and  $\gamma$ , all of which are estimated using a dual filter.

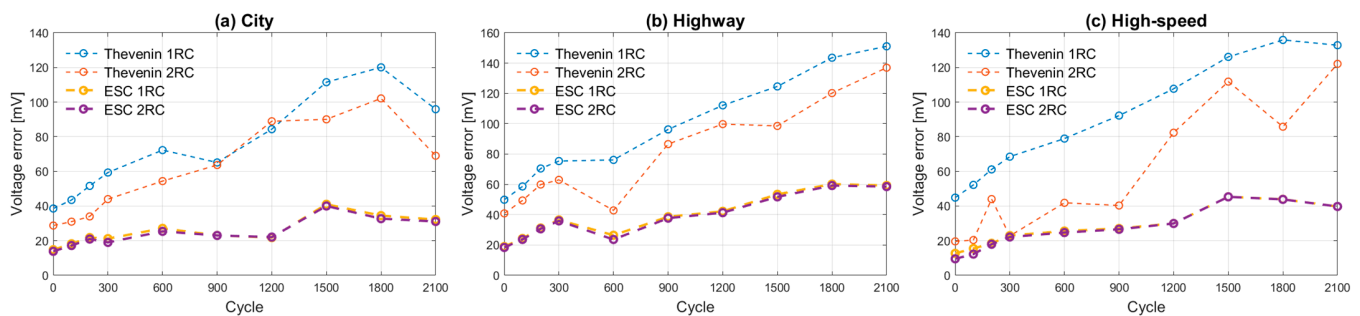


**Figure 5.** Variations in terminal voltage predictions over cycles under (a) City, (b) Highway, and (c) High-speed profiles.

The estimated values of  $z$  and  $Q$  were compared against their true values obtained using the current sensors integrated in the test equipment. This dedicated sensor was designed for ultra-high precision measurement of currents, ensuring an accuracy of less than 0.01% across all measurement ranges. Although typical current sensors in commercial BMSs operate with single-digit accuracy around 3%, we aim to improve upon these less reliable measurements with estimates derived from the developed cell model and its filter.

#### 4. Dual Filtering

This section formulates the DEKF and applies it to simultaneously estimate the states and parameters during battery aging. Among the parameters, the present capacity was solely estimated using a separate optimization technique due to its poor observability in the developed filter.

Fundamentally, the KF serves as the optimal state estimator, if the considered system is linear and the uncertainties are represented by Gaussian random variables. If the system is not linear, a linearization process is performed at every time step to approximate the nonlinear system as a linear time-varying system. The linearized system can then be utilized within the KF framework, generating the EKF that operates on the original nonlinear system. The original nonlinear system is in the form of a state-space model that describes the dynamics of states:

$$x_k = f(x_{k-1}, u_{k-1}) + \omega_{k-1} \quad (3)$$

$$y_k = g(x_k, u_k) + v_k \quad (4)$$

where  $\omega_k$  is the process noise with the covariance matrix  $\Sigma_\omega$ , and  $v_k$  is the measurement noise with the covariance matrix  $\Sigma_v$ . Here,  $f$  is a nonlinear state transition function, and  $g$  is a nonlinear measurement function.

The EKF uses this system model in a recursive process to update its estimate of the present state. The two steps, time update (prediction) and measurement update, are

performed repeatedly, as follows. Note that  $x^-$  denotes a predicted value,  $x^+$  denotes an updated value,  $\hat{x}$  denotes an estimated value, and  $\Sigma_x$  denotes the covariance of  $\hat{x}$ . Initially, the present state is predicted given the past state estimate and the system input:

$$\hat{x}_k^- = f(\hat{x}_{k-1}^+, u_{k-1}) \quad (5)$$

Next, the uncertainty of the state estimate is predicted:

$$\Sigma_{x,k}^- = A_{k-1} \Sigma_{x,k-1}^+ A_{k-1}^T + \Sigma_\omega \quad (6)$$

From here, the measurement update is followed by the time update. The measurements of the system output are taken and compared to the predictions derived from the state estimate:

$$\hat{x}_k^+ = \hat{x}_k^- + L_k (y_k - g(\hat{x}_k^-, u_k)) \quad (7)$$

The state estimate is updated based on the prediction error and the Kalman gain. The Kalman gain is computed based on the sensitivity of the output to various states (represented by the Jacobian matrix in the EKF) and the uncertainty of the states (represented by the error covariance matrix):

$$L_k = \Sigma_{x,k}^- C_k^T (C_k \Sigma_{x,k}^- C_k^T + \Sigma_v)^{-1} \quad (8)$$

Subsequently, the uncertainty of the state estimate is updated:

$$\Sigma_{x,k}^+ = (I - L_k C_k) \Sigma_{x,k}^- \quad (9)$$

The original nonlinear system within the EKF refers to the cell model developed in Section 3. The states in the model, SOC as an example, can change rapidly over time, spanning its entire range within several minutes. In contrast, the model parameters, such as capacity, change slowly. The SOC generally denotes the residual capacity with respect to the present capacity, leading to a strong correlation between them. Therefore, we devised the DEKF based on two separate but cooperating filters: the state filter and parameter filter [39,40]. While the state filter remains consistent with Equations (3) and (4), the parameter filter introduces a new state-space model that describes the dynamics of parameters:

$$\theta_k = \theta_{k-1} + r_{k-1} \quad (10)$$

$$d_k = g(x_k, u_k, \theta_k) + e_k \quad (11)$$

where  $r_k$  is the process noise and  $e_k$  is the measurement noise. According to Equation (10), the parameters are essentially constant, but they may change slowly with respect to time and are modeled by a fictitious process noise. Each filter executes the aforementioned process to estimate either the states or the parameters, and they are linked by exchanging information during the time update step.

This interconnected process enables the more accurate tracking of changes in the states and parameters, with the exception of the present capacity. The weak observability of capacity has also been reported [32,41]. Here, the DEKFs have difficulty accurately estimating capacity. This observation is related to the facts that the terminal voltage is the sole measurement, and capacity is weakly linked to the terminal voltage, according to the derived system model. This inaccuracy in capacity estimation can also negatively impact SOC estimation, owing to its strong dependency on the present capacity.

Specifically for capacity estimation, the parameter filter of the developed DEKF was thus replaced with a separate optimization technique based on the weighted least-squares (WLS). As reported in series [42–44], this method has been continuously improved, aiming at its BMS implementation. The basis of this method is to estimate the present capacity in the least-squares sense by utilizing changes in the shape of a charge curve as capacity



decreases. The present capacity is estimated during battery charging, taking advantage of highly standardized and less dynamic charging profiles compared to arbitrary discharging profiles. In practice, however, the shape of the curve is influenced by operational factors before charging; for example, the duty cycle, rest time, SOC, and temperature. The WLS was thus selected to assign varying weights to each data point on the curve, since they differ in reliability for capacity estimation. In consequence, the WLS assigns greater weights to the later part of the curve, as these points are more dependable than those in the earlier part. Despite variations in such operational factors, a capacity error of less than 3% was achieved. However, this original scheme relies on prior information, specifically the past capacity estimate, which serves as the best guess for the true value of the present capacity. Consequently, if batteries or their BMSs are replaced, the stored value of capacity in the BMS no longer matches the actual value. The original scheme is enhanced to eliminate this issue, allowing it to operate independently of such replacements. Meanwhile, the original scheme relies on the WLS as its optimization technique, which necessitates Jacobian calculations and matrix inversion to solve the normal equation. As a result, during batch processing, state estimation requires substantially higher CPU usage and greater memory capacity than data measurement, creating challenges for BMS implementation. The original scheme is enhanced to mitigate these issues by replacing the batch estimator with a recursive estimator for solving the normal equation. This replacement helps distribute CPU usage more evenly and reduces the memory footprint since it eliminates the need for long, multi-vector formulations of the normal equation. By adopting this method, the present capacity was solely estimated during charging, while the states and the remaining parameters were simultaneously estimated by the DEKF during discharging.

## 5. Filter Validation

This section validates the developed filter using the test data collected during battery aging. As described in Section 2, a total of 30 datasets were provided for this validation. These datasets encompassed the three load profiles applied to ten aged cells. The lowest capacity among these cells was 2.254 Ah, which is equivalent to less than 70% SOH. The validation result refers to an error between the estimated and measured values. As described in Section 3, the ESC 1RC model created by averaging the parameters derived from the three load profiles was used for this validation. Compared to the Thevenin model, the ESC model provided greater fidelity to the battery aging test data, primarily due to the inclusion of a hysteresis element that captured changes in the SOC-OCV curve with battery aging. This result implies that the key aging-related parameters include  $R_0$ , which reflects an increase in internal resistance, and  $M$  and  $M_0$ , which represent alterations in the SOC-OCV relationship within the hysteresis element. In this study, a mean value (RMSE) was used to evaluate SOC estimates, whereas a final value was used for capacity estimates. Their measurements were commonly based on Coulomb counting with current sensors enhanced with internal compensation.

Based on the validation result, we developed three different schemes successively, as illustrated in Figure 6. The first scheme relies solely on the simultaneous estimator to concurrently update the SOC and capacity, leading to inaccuracy in capacity estimation. To address this issue in the DEKF, the second scheme substitutes its parameter filter for capacity estimation with the WLS. Despite having this separate capacity estimator, maintaining accuracy during battery aging is still challenging. As an effective alternative, the third scheme repeats the sequential estimator to intermittently update all the model parameters. In the first and second schemes, this parameter identification for cell modeling is performed only once with a fresh cell, as described in Section 3. Figure 7 compares the sequential and simultaneous estimators in detail.

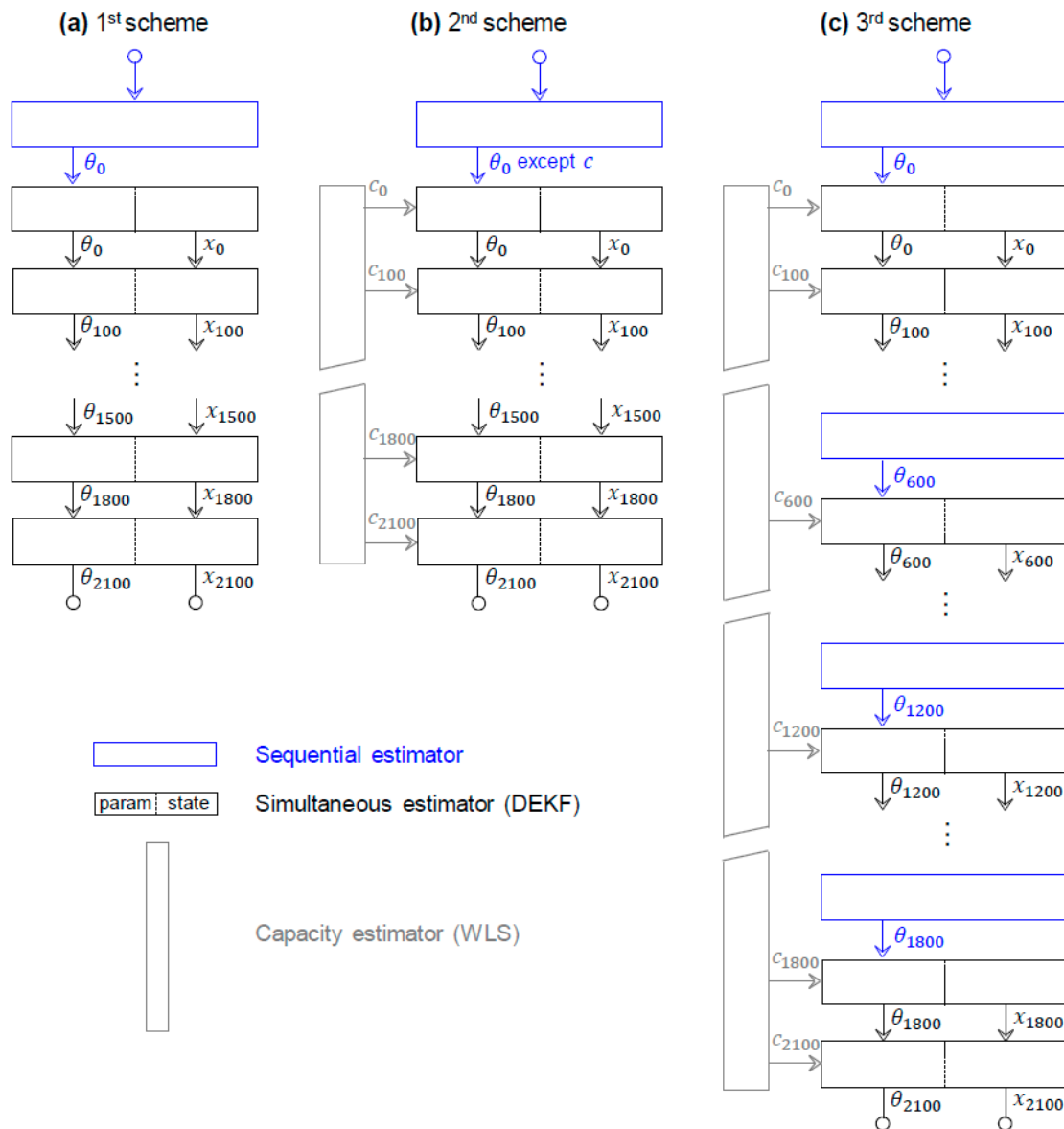


**Figure 6.** Comparison between the three schemes developed.

### 5.1. First Scheme

As a result of the first scheme, Figure 8 presents the SOC error, comparing estimation accuracy across the type of load profiles and the number of cycles. Regarding the effect of cycle number, the SOC error generally increases as capacity decreases, except at cycle 1500. The test performed at this cycle is considered flawed because a similar anomaly is also observed in Figure 2, which shows changes in the rated capacity. The cycles earlier than 900 exhibit an RMSE of less than 3%, regardless of load type. However, the error exceeds 3% and rises rapidly from cycle 900 onward, where the SOH reaches nearly 80%. Regarding the effect of load type, the SOC error remains similar across each type until cycle 1200. From this cycle, except for cycle 1500, the increasing error in the City model is less severe than in other models based on more aggressive load profiles. The SOC error in this model remains within 5% throughout all cycles. Capacity reduction necessarily accompanies an increase in internal resistance. Due to this increase, higher C-rates in the Highway and High-speed profiles cause greater voltage drops, particularly in more aged cells. As a result, the inability to accurately predict fluctuations in the terminal voltage leads to poor SOC estimation, which is more severe at low SOC levels towards the end of the load profile.

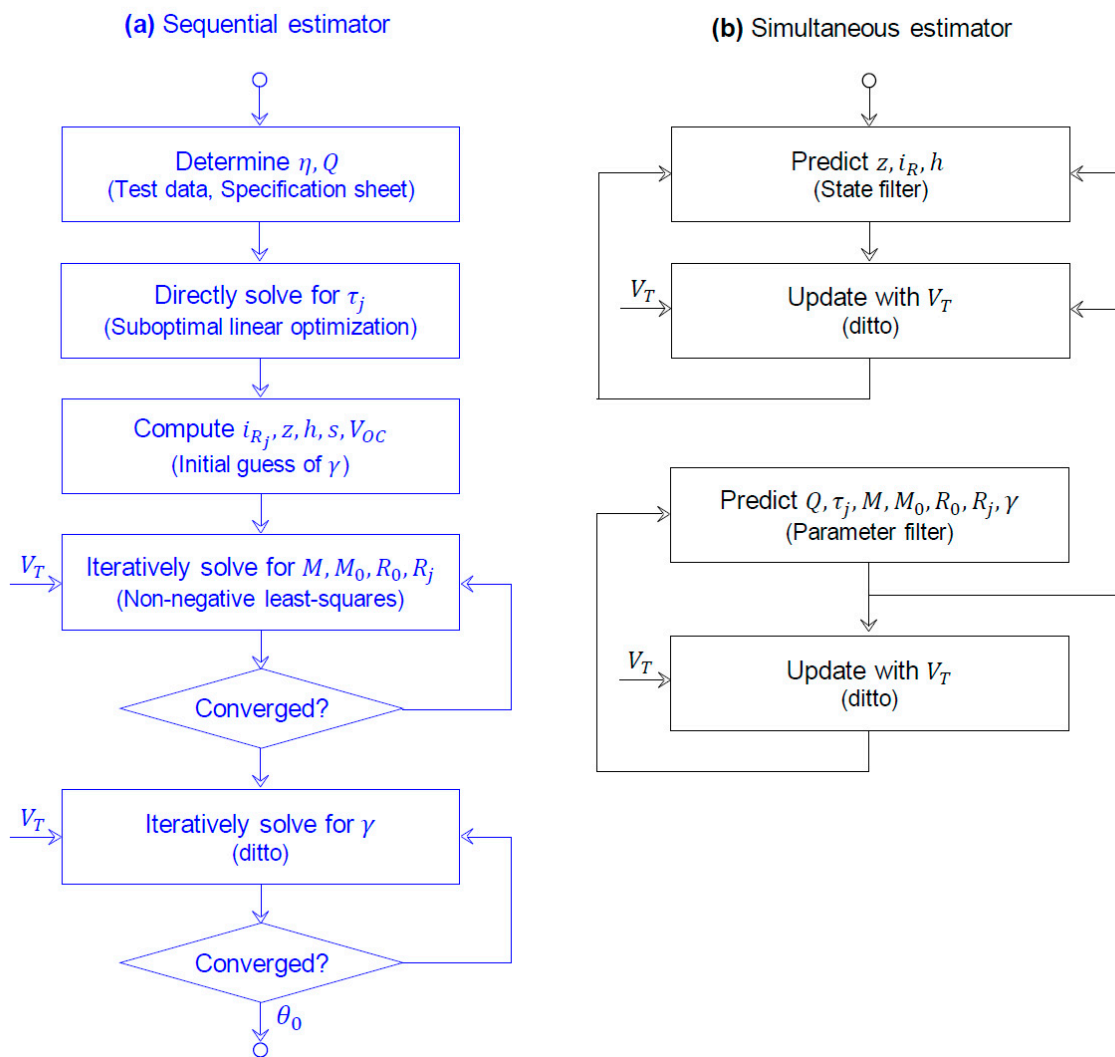


**Figure 7.** Comparison of the (a) sequential and (b) simultaneous estimators.

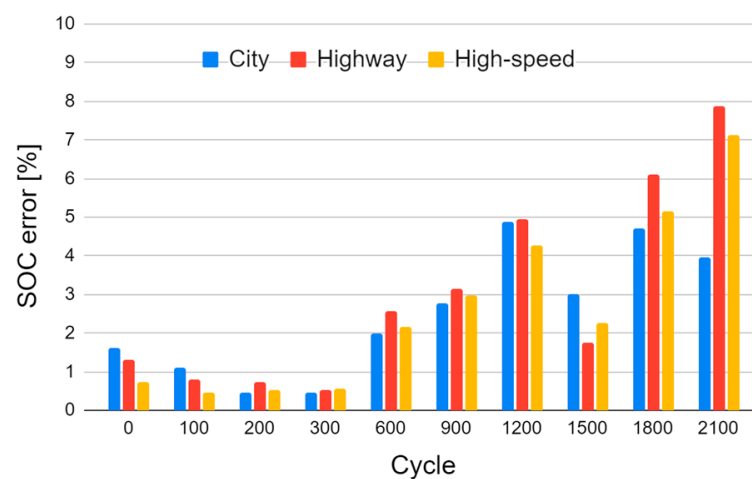


**Figure 8.** Variations in SOC estimates (error) over cycles in the first scheme.

This inference can be confirmed in Figure 9, which plots changes in the SOC error with its bounds against time, comparing estimation accuracy across the types of load profiles and the number of cycles. Due to space constraints, the estimation results from five specific cycles (0, 600, 1200, 1800, and 2100) are selectively displayed. The impact of an initial

SOC on tracking performance is as significant as that of the cycle number. Here, some initial values are not visible because of the unified range of SOC error ( $-5\sim 5\%$ ) across 12 cases. To address this lack of prior information, Table 2 lists the initial SOC estimates for each load profile and cycle number. In this study, the initial SOC was determined using the SOC-OCV curve, assuming that the terminal voltage converges to the OCV after long enough relaxation periods. To mimic the actual operations of PHEVs, the test involves resting after charging to 90% SOC, as described in Section 2. In the earlier cycles, the initial SOC is commonly estimated to be 88%, resulting in an SOC error of about 2%. Similar to the mean value (RMSE) of SOC in Figure 8, the error in its initial value increases as capacity decreases, regardless of model type. This observation suggests that the curve established for a fresh cell loses effectiveness because of the physicochemical changes in aged cells. This inference was also made in Section 3, and the current results provide even stronger evidence.

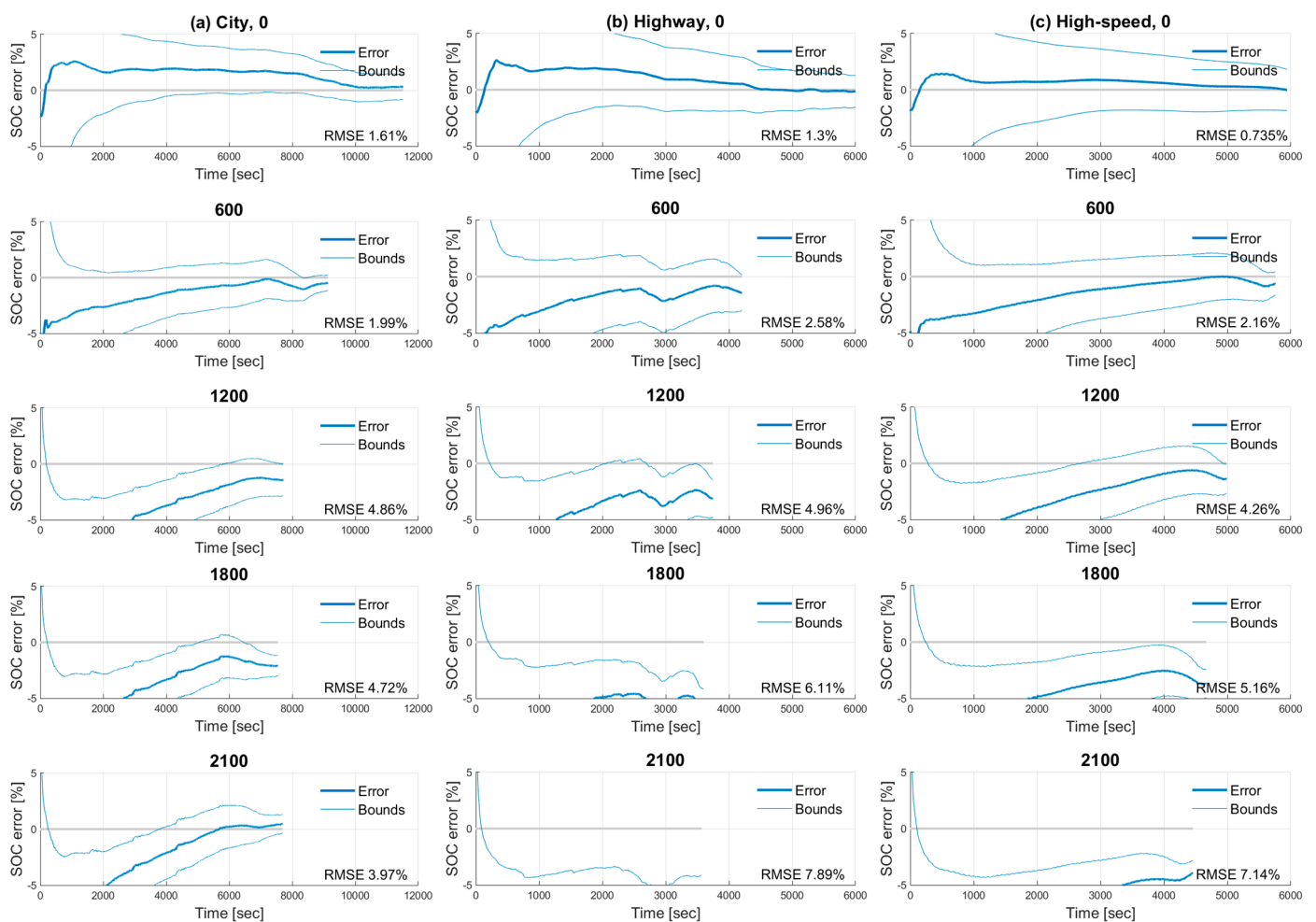


**Figure 9.** Variations in SOC estimates (error) over time under (a) City, (b) Highway, and (c) High-speed profiles.

**Table 2.** Initial SOC estimates.

Cycle	0	100	200	300	600	900	1200	1500	1800	2100
City	0.88	0.88	0.87	0.87	0.85	0.84	0.81	0.81	0.79	0.79
Highway	0.88	0.88	0.88	0.87	0.85	0.83	0.82	0.82	0.8	0.78
High-speed	0.88	0.88	0.88	0.87	0.85	0.83	0.82	0.83	0.8	0.78

As another result of the first scheme, Figure 10 plots changes in the measured and estimated capacities, comparing estimation accuracy across the type of load profiles and the number of cycles. The measurements are consistent with those in Figure 2. The resulting estimates are consistent with our concerns about the weak observability of capacity in the DEKF, as discussed in Section 4. This inaccuracy in capacity estimation can adversely affect SOC estimation, due to its direct relation to the present capacity. This claim is supported by the fact that, although there are slight differences depending on load type, the capacity estimation error generally starts to increase after 600 cycles, following the same trend as the SOC estimation results, as presented in Figure 8. Therefore, from the next scheme, capacity is updated separately from the simultaneous estimator.

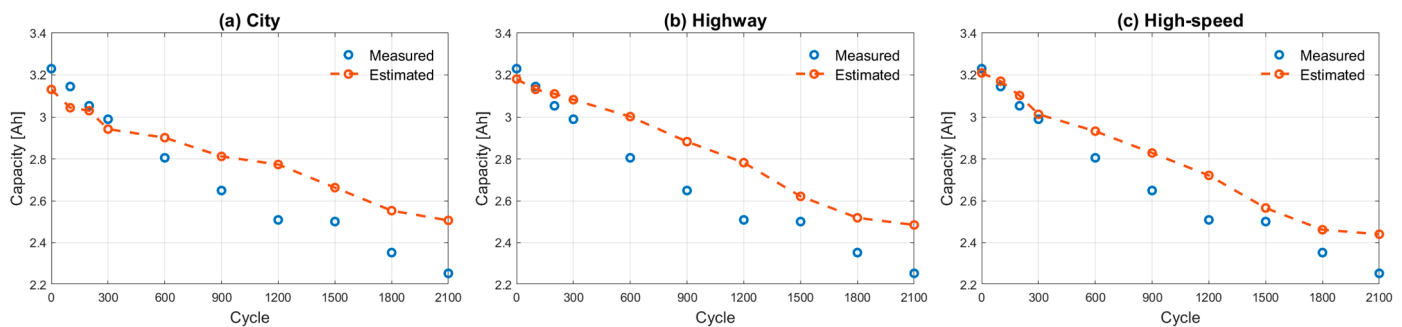


**Figure 10.** Variations in capacity estimates over cycles in the first scheme based on the (a) City, (b) Highway, and (c) High-speed profiles.

### 5.2. Second Scheme

As a consequence of the second scheme, Figure 11 plots changes in the measured and estimated capacities, comparing estimation accuracy across the number of cycles. Unlike the first scheme, the present capacity is estimated during battery charging, corresponding to one single load type. This load profile is simply based on constant power charging at 9 W until the SOC reaches 90%, reflecting the real-world operations of PHEVs. By decoupling capacity estimation from the parameter filter of the DEKF, an estimation error within 3% can be realized, as witnessed in [42].

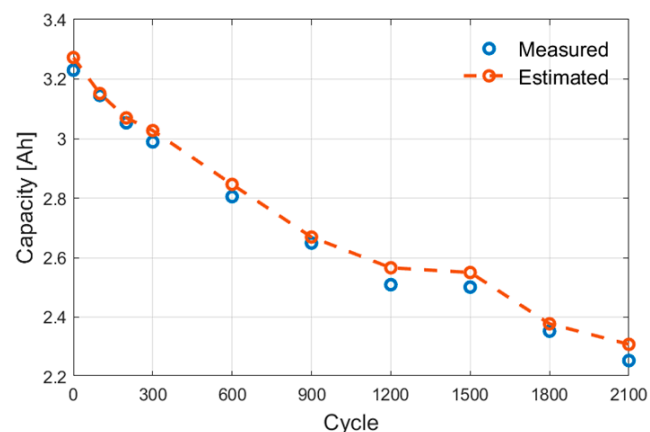


**Figure 11.** Variations in capacity estimates over cycles in the second scheme based on the constant power charging profile.

Figure 12 presents the SOC error, comparing estimation accuracy across the type of load profiles and the number of cycles. The resulting estimates are comparable to those in Figure 8, which is derived from the first scheme. Unfortunately, despite notable improvement in capacity accuracy, no corresponding enhancement is observed in the SOC. The SOC error is actually worse than in the first scheme, yielding RMSEs exceeding 5%

after 600 cycles. Despite having capacities close to their true values, the decline is persistent. Compared to the cell model, its filter is much more responsible for this inaccuracy in SOC estimation. This is because, as demonstrated in Figure 5, the ESC 1RC model can only retain accuracy within a certain range if its parameters are properly identified using the sequential estimator. Therefore, in the next scheme, all the model parameters except for capacity are updated intermittently with the sequential estimator.

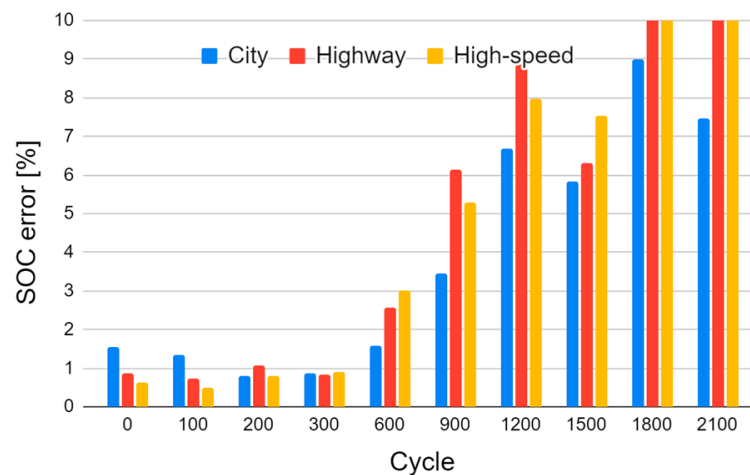


**Figure 12.** Variations in SOC estimates (error) over cycles in the second scheme.

### 5.3. Third Scheme

As a result of the third scheme, Figure 13 presents the SOC error, comparing estimation accuracy across the type of load profiles and the number of cycles. The resulting estimates are comparable to those in Figures 8 and 12, which are derived from the first and second schemes, respectively. As discussed in Section 3, the sequential estimator is tailored to effectively extract multiple parameters in the ESC model using a single measurement. In place of the typical parameter filter in the simultaneous estimator, this method is applied prior to performing cycles 600, 1200, and 1800, where the SOC error starts to rise rapidly. As also shown in Figure 14, an increase in SOC error is effectively suppressed, maintaining an accuracy within 5% throughout all the cycles.

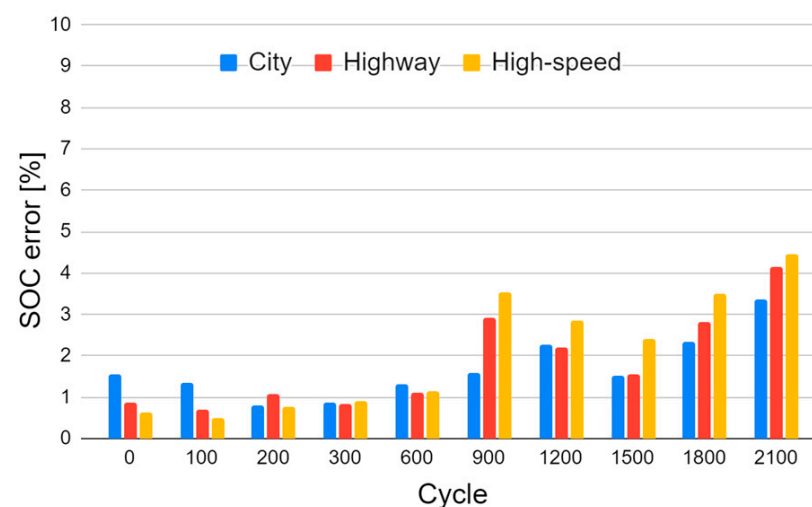


**Figure 13.** Variations in SOC estimates (error) over cycles in the third scheme.



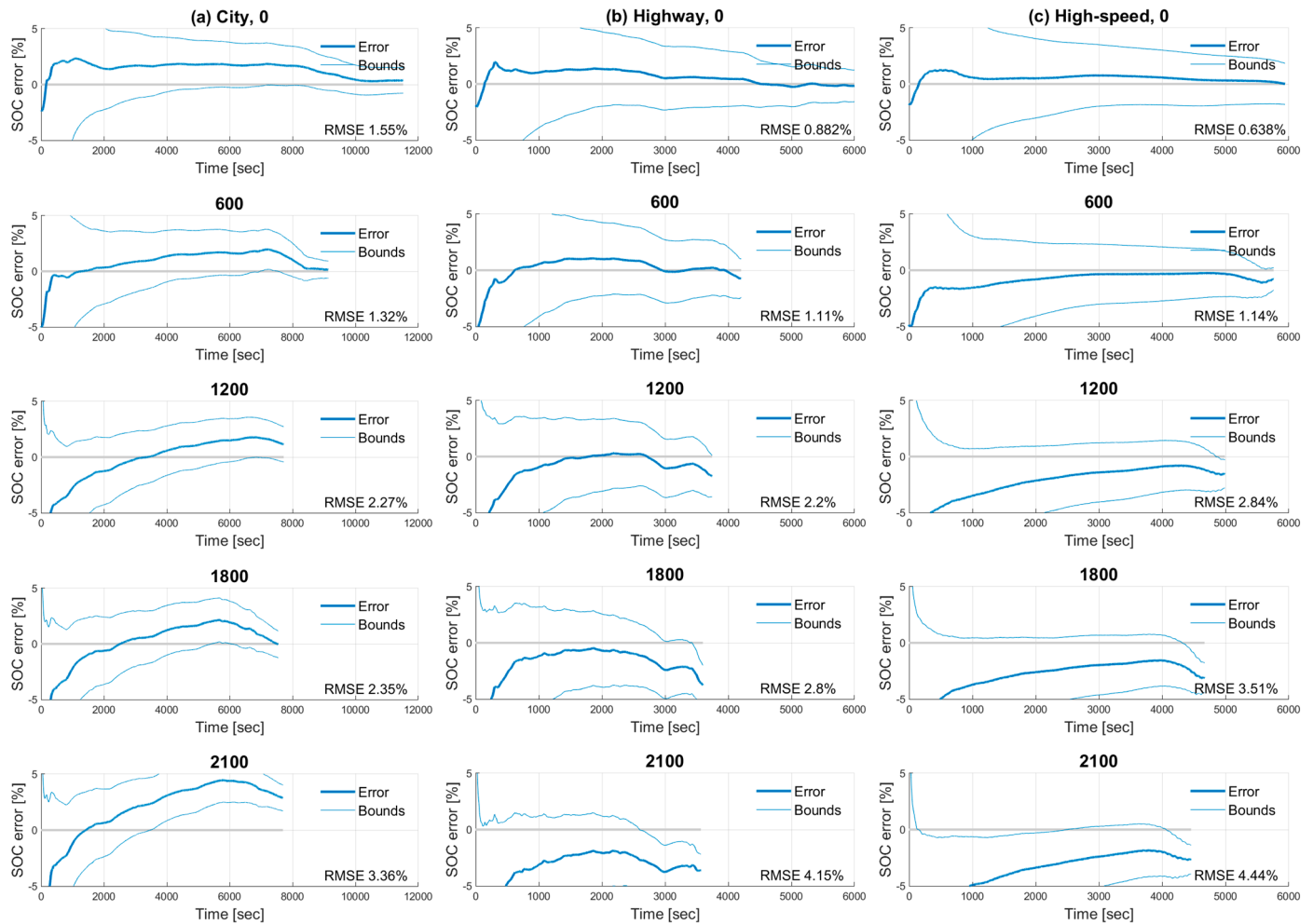


**Figure 14.** Variations in SOC estimates (error) over time under (a) City, (b) Highway, and (c) High-speed profiles.

## 6. Conclusions

This paper serves as a sequel to our previous study. In our original paper [37], the effect of current sensor bias on SOC accuracy was studied. Subsequently, the effect of changes in capacity was studied in this paper. For maintaining SOC estimation accuracy despite battery aging, the present capacity needs to be properly updated. To efficiently adapt model parameters, including capacity, to the physicochemical changes in aged cells, the simultaneous estimator was developed based on the DEKF (first scheme). However, the parameter filter in the DEKF suffered from a weak observability of its capacity, which we believe is responsible for the inaccurate SOC, particularly noticeable beyond 600 cycles. The present capacity was therefore updated using a separate estimator based on the WLS (second scheme), but it proved ineffective. We speculated that the less accurate SOC, especially when the SOH drops by more than 10%, was not caused by the capacity parameter alone, but rather that all parameters were not updated properly. To this end, the model parameters were reset intermittently in a similar way as they were initialized using the sequential estimator (third scheme). Despite a 30% decrease in SOH, the target SOC accuracy of 5% was achieved through the sequential estimator. The three schemes are summarized and compared in Table 3.

**Table 3.** Comparison of the three schemes designed for co-estimating SOC and capacity.

Scheme		1	2	3
Max estimation error [%]	SOC	7.9	11.8	4.4
	Capacity	11.2	2.4	2.4
Robustness under aging		Good	Fair	Excellent
BMS implementation		Good	Fair	Poor
Advantage		Simple implementation	Improved capacity accuracy	Best overall accuracy and robustness
Disadvantage		Higher error in later cycles	Slightly increased complexity	Most complex implementation

Throughout this trial and error, several issues emerged that were not addressed in previous studies [31–35]. The conclusion and future work of this study are summarized as follows:

- Compared to the Thevenin model, the ESC model offers higher fidelity to the battery aging test data. At the cost of the added hysteresis element, changes in the SOC-OCV curve with battery aging can be modeled, albeit unintentionally.
- To fully leverage the potential of the ESC model, however, a dedicated parameter identification scheme for this model, such as the sequential estimator, is essential.
- In practice, applying the sequential estimator to BMSs operating in real time, including iterative solvers with unpredictable convergence times, requires further works.
- If changes in the SOC-OCV curve can be identified with BMSs operating on board, using a relatively simple model like the Thevenin model and updating the curve at appropriate intervals could serve as an alternative to the current approach.

**Author Contributions:** Conceptualization, W.S. and J.-H.C.; methodology, M.Y.Y.; software, M.Y.Y. and J.H.L.; validation, M.Y.Y. and J.H.L.; investigation, J.H.L. and H.L.; writing—original draft preparation, M.Y.Y.; writing—review and editing, W.S. and J.-H.C.; supervision, W.S.; project administration, J.S.H.; funding acquisition, J.S.H. All authors have read and agreed to the published version of the manuscript.

**Funding:** This work was supported by the “Technology development of hybrid electric propulsion systems for manned future air mobility” program (1711170902) by Korea Aerospace Research Institute, Republic of Korea.

**Data Availability Statement:** The raw data supporting the conclusions of this article will be made available by the authors on request.

**Conflicts of Interest:** The authors declare no conflicts of interest.

## References

1. Zubi, E.G.; Dufo-López, R.; Carvalho, M.; Pasaoglu, G. The lithium-ion battery: State of the art and future perspectives. *Renew. Sustain. Energy Rev.* **2018**, *89*, 292–308. [\[CrossRef\]](#)
2. Zeng, X.; Li, J.; Singh, N.; Wang, Y.; Dong, S.; Zhang, T. Recycling of spent lithium-ion battery for recovery of valuable metals: A critical review. *Batteries* **2023**, *9*, 64.
3. Xing, Y.; Ma, E.W.M.; Tsui, K.L.; Pecht, M. Battery management systems in electric and hybrid vehicles. *Energies* **2011**, *4*, 1840–1857. [\[CrossRef\]](#)
4. Shrivastava, P.; Soon, T.K.; Idris, M.Y.I.B.; Mekhilef, S. Overview of model-based online state-of-charge estimation using Kalman filter family for lithium-ion batteries. *Renew. Sustain. Energy Rev.* **2019**, *113*, 109233. [\[CrossRef\]](#)
5. Ali, M.U.; Zafar, A.; Nengroo, S.H.; Hussain, S.; Alvi, M.J.; Kim, H.-J. Towards a smarter battery management system for electric vehicle applications: A critical review of lithium-ion battery state of charge estimation. *Energies* **2019**, *12*, 446. [\[CrossRef\]](#)
6. Park, S.; Ahn, J.; Kang, T.; Park, S.; Kim, Y.; Cho, I.; Kim, J. Review of state-of-the-art battery state estimation technologies for battery management systems of stationary energy storage systems. *J. Power Electron.* **2020**, *20*, 1526–1540. [\[CrossRef\]](#)
7. Khan, Z.A.; Shrivastava, P.; Amrr, S.M.; Mekhilef, S.; Algethami, A.A.; Seyedmahmoudian, M.; Stojcevski, A. A comparative study on different online state of charge estimation algorithms for lithium-ion batteries. *Sustainability* **2022**, *14*, 7412. [\[CrossRef\]](#)

8. Hannan, M.A.; Lipu, M.S.H.; Hussain, A.; Mohamed, A. A review of lithium-ion battery state of charge estimation and management system in electric vehicle applications: Challenges and recommendations. *Renew. Sustain. Energy Rev.* **2017**, *78*, 834–854. [\[CrossRef\]](#)
9. How, D.N.T.; Hannan, M.A.; Lipu, M.S.H.; Ker, P.J. State of charge estimation for lithium-ion batteries using model-based and data-driven methods: A review. *IEEE Access* **2019**, *7*, 136116–136136. [\[CrossRef\]](#)
10. Shi, Q.; Jiang, Z.; Wang, Z.; Shao, X.; He, L. State of charge estimation by joint approach with model-based and data-driven algorithm for lithium-ion battery. *IEEE Trans. Instrum. Meas.* **2022**, *71*, 1–10. [\[CrossRef\]](#)
11. Wang, Z.; Feng, G.; Zhen, D.; Gu, F.; Ball, A. A review on online state of charge and state of health estimation for lithium-ion batteries in electric vehicles. *Energy Rep.* **2021**, *7*, 5141–5164. [\[CrossRef\]](#)
12. Hossain, M.; Haque, M.; Arif, M. Kalman filtering techniques for the online model parameters and state of charge estimation of the li-ion batteries: A comparative analysis. *J. Energy Storage* **2022**, *51*, 1–15. [\[CrossRef\]](#)
13. Plett, G.L. Extended Kalman filtering for battery management systems of LiPB-based HEV battery packs: Part 3. State and parameter estimation. *J. Power Sources* **2004**, *134*, 277–292. [\[CrossRef\]](#)
14. Plett, G.L. Sigma-point Kalman filtering for battery management systems of LiPB-based HEV battery packs. Part 1: Introduction and state estimation. *J. Power Sources* **2006**, *161*, 1356–1368. [\[CrossRef\]](#)
15. Lee, S.; Kim, J.; Lee, J.; Cho, B.H. State-of-charge and capacity estimation of lithium-ion battery using a new open-circuit voltage versus state-of-charge. *J. Power Sources* **2008**, *185*, 1367–1373. [\[CrossRef\]](#)
16. Hu, C.; Youn, B.D.; Chung, J. A multiscale framework with extended Kalman filter for lithium-ion battery SOC and capacity estimation. *Appl. Energy* **2012**, *92*, 694–704. [\[CrossRef\]](#)
17. Zhang, X.; Wang, Y.; Yang, D.; Chen, Z. An on-line estimation of battery pack parameters and state-of-charge using dual filters based on pack model. *Energy* **2016**, *115*, 219–229. [\[CrossRef\]](#)
18. Campestrini, C.; Heil, T.; Kosch, S.; Jossen, A. A comparative study and review of different Kalman filters by applying an enhanced validation method. *J. Energy Storage* **2016**, *8*, 142–159. [\[CrossRef\]](#)
19. Guo, H.; Wang, Z.; Li, Y.; Wang, D.; Wang, G. State of charge and parameters estimation for Lithium-ion battery using dual adaptive unscented Kalman filter. In Proceedings of the 2017 29th Chinese Control and Decision Conference (CCDC), Chongqing, China, 28–30 May 2017; pp. 4962–4966.
20. Zeng, M.; Zhang, P.; Yang, Y.; Xie, C.; Shi, Y. SOC and SOH joint estimation of the power batteries based on fuzzy unscented Kalman filtering algorithm. *Energies* **2019**, *12*, 3122. [\[CrossRef\]](#)
21. Lai, X.; He, L.; Wang, S.; Zhou, L.; Zhang, Y.; Sun, T.; Zheng, Y. Co-estimation of state of charge and state of power for lithium-ion batteries based on fractional variable-order model. *J. Clean. Prod.* **2020**, *255*, 120203. [\[CrossRef\]](#)
22. Shrivastava, P.; Soon, T.K.; Idris, M.Y.I.B.; Mekhilef, S.; Adnan, S.B.R.S. Comprehensive co-estimation of lithium-ion battery state of charge, state of energy, state of power, maximum available capacity, and maximum available energy. *J. Energy Storage* **2022**, *56*, B106049. [\[CrossRef\]](#)
23. Guo, R.; Shen, W. A model fusion method for online state of charge and state of power co-estimation of lithium-ion batteries in electric vehicles. *IEEE Trans. Veh. Technol.* **2022**, *71*, 11515–11525. [\[CrossRef\]](#)
24. Li, K.; Gao, X.; Liu, C.; Chang, C.; Li, X. A novel co-estimation framework of state-of-charge, state-of-power and capacity for lithium-ion batteries using multi-parameters fusion method. *Energy* **2023**, *269*, 126820. [\[CrossRef\]](#)
25. Ye, L.; Peng, D.; Xue, D.; Chen, S.; Shi, A. Co-estimation of lithium-ion battery state-of-charge and state-of-health based on fractional-order model. *J. Energy Storage* **2022**, *65*, 107225. [\[CrossRef\]](#)
26. Zhang, R.; Li, X.; Sun, C.; Yang, S.; Tian, Y.; Tian, J. State of Charge and Temperature Joint Estimation Based on Ultrasonic Reflection Waves for Lithium-Ion Battery Applications. *Batteries* **2023**, *9*, 335. [\[CrossRef\]](#)
27. Sepasi, S.; Ghorbani, R.; Liaw, B.Y. A novel on-board state-of-charge estimation method for aged Li-ion batteries based on model adaptive extended Kalman filter. *J. Power Sources* **2014**, *245*, 337–344. [\[CrossRef\]](#)
28. Shen, P.; Ouyang, M.; Lu, L.; Li, J.; Feng, X. The co-estimation of state of charge state of health and state of function for lithium-ion batteries in electric vehicles. *IEEE Trans. Veh. Technol.* **2018**, *67*, 92–103. [\[CrossRef\]](#)
29. Li, X.; Wang, Z.; Zhang, L. Co-estimation of capacity and state-of-charge for lithium-ion batteries in electric vehicles. *Energy* **2019**, *174*, 33–44. [\[CrossRef\]](#)
30. Xu, Z.; Wang, J.; Lund, P.; Zhang, Y. Co-estimating the state of charge and health of lithium batteries through combining a minimalist electrochemical model and an equivalent circuit model. *Energy* **2022**, *240*, 122815. [\[CrossRef\]](#)
31. Xiong, R.; Sun, F.; Chen, Z.; He, H. A data-driven multi-scale extended Kalman filtering based parameter and state estimation approach of lithium-ion polymer battery in electric vehicles. *Appl. Energy* **2014**, *113*, 463–476. [\[CrossRef\]](#)
32. Wassiliadis, N.; Adermann, J.; Frericks, A.; Pak, M.; Reiter, C.; Lohmann, B.; Lienkamp, M. Revisiting the dual extended Kalman filter for battery state-of-charge and state-of-health estimation: A use-case life cycle analysis. *J. Energy Storage* **2018**, *19*, 73–87. [\[CrossRef\]](#)
33. Wu, J.; Jiao, C.; Chen, M.; Chen, J.; Zhang, Z. SOC Estimation of Li-ion Battery by Adaptive Dual Kalman Filter under Typical Working Conditions. In Proceedings of the 2019 IEEE 3rd International Electrical and Energy Conference (CIEEC), Beijing, China, 7–9 September 2019; pp. 1561–1567.
34. Hu, X.; Yuan, H.; Zou, C.; Li, Z.; Zhang, L. Co-estimation of state of charge and state of health for lithium-ion batteries based on fractional-order calculus. *IEEE Trans. Veh. Technol.* **2018**, *67*, 10319–10329. [\[CrossRef\]](#)

35. Ma, L.; Xu, Y.; Zhang, H.; Yang, F.; Wang, X.; Li, C. Co-estimation of state of charge and state of health for lithium-ion batteries based on fractional-order model with multi-innovations unscented Kalman filter method. *J. Energy Storage* **2022**, *52*, 104904. [[CrossRef](#)]
36. Zhu, M.; Wang, Y.; Shi, P. Robust Kalman Filtering Under Model Uncertainty: The Case of Degenerate Densities. *IEEE Trans. Autom. Control* **2021**, *66*, 5198–5205.
37. Yoo, M.Y.; Lee, J.H.; Sung, W.; Huh, J.S.; Choi, J.H. State-of-Charge Estimation of Batteries for Hybrid Urban Air Mobility. *Aerospace* **2023**, *10*, 550. [[CrossRef](#)]
38. Plett, G.L. *Battery Management Systems, Volume 1: Battery Modeling*; Artech House: Norwood, MA, USA, 2015.
39. Plett, G.L. *Battery Management Systems, Volume 2: Equivalent-Circuit Methods*; Artech House: Norwood, MA, USA, 2015.
40. Plett, G.L. Dual and joint EKF for simultaneous SOC and SOH estimation. In Proceedings of the 21st Electric Vehicle Symposium (EVS21), Monte Carlo, Monaco, 2–6 April 2005; pp. 1–12.
41. Lecture Notes and Recordings for ECE4710/5710: Modeling, Simulation, and Identification of Battery Dynamics. Available online: <http://mocha-java.uccs.edu/ECE5710/index.html> (accessed on 20 February 2023).
42. Sung, W.; Nam, J.; Choi, J.H.; Lee, J. Robust and efficient capacity estimation using data-driven metamodel applicable to battery management system of electric vehicles. *J. Electrochem. Soc.* **2016**, *163*, A981. [[CrossRef](#)]
43. Sung, W.; Lee, J. Improved capacity estimation technique for the battery management systems of electric vehicles using the fixed-point iteration method. *Comput. Chem. Eng.* **2018**, *117*, 283–290. [[CrossRef](#)]
44. Sung, W.; Lee, J. Implementation of SOH estimator in automotive BMSs using recursive least-squares. *Electronics* **2019**, *8*, 1237. [[CrossRef](#)]

**Disclaimer/Publisher’s Note:** The statements, opinions and data contained in all publications are solely those of the individual author(s) and contributor(s) and not of MDPI and/or the editor(s). MDPI and/or the editor(s) disclaim responsibility for any injury to people or property resulting from any ideas, methods, instructions or products referred to in the content.